Peer reviewed version

Link to published version (if available):
10.1021/acs.nanolett.7b04995

Link to publication record in Explore Bristol Research
PDF-document

University of Bristol - Explore Bristol Research
General rights

Dual Control of Molecular Conductance through pH and Potential in Single-Molecule Devices.

Richard J. Brooke[†], Doug S. Szumski[†], Andrea Vezzoli[‡], Simon J. Higgins[‡], Richard J. Nichols[‡] and Walther Schwarzacher[†]*

[†] H. H. Wills Physics Laboratory, University of Bristol, Tyndall Avenue, Bristol BS8 1TL, UK.

[‡] Department of Chemistry, University of Liverpool, Crown Street, Liverpool L69 7ZD, UK.

ABSTRACT

One of the principal aims of single-molecule electronics is to create practical devices out of individual molecules. Such devices are expected to play a particularly important role as novel sensors thanks to their response to wide ranging external stimuli. Here we show that the conductance of a molecular junction can depend on two independent stimuli simultaneously. Using a scanning tunnelling microscope break-junction technique (STM-BJ), we found that the conductance of 4,4'-vinylenedipyridine (44VDP) molecular junctions with Ni contacts depends on both the electrochemically applied gate voltage and the pH of the environment. Hence, not only can the Ni|44VDP|Ni junction function as a pH-sensitive switch, but the value of the pH at which switching takes place can be tuned electrically. Furthermore, through the simultaneous control of pH and potential the STM-BJ technique delivers unique insight into the acid-base reaction, including the observation of discrete proton transfers to and from a single molecule.

KEYWORDS: break-junction, molecular electronics, electron transfer, sensors, protonation, fluctuations

MAIN TEXT

Future electronic devices in which individual molecules provide functionality may deliver unparalleled miniaturization and easily tailored electronic behaviour through chemical design. For example, single-molecule devices such as transistors[1–3], current rectifiers[4–7] and interconnecting wires[8,9] have all been identified. Such devices can also be sensitive to a variety of external stimuli[7,8,10–15] and are expected to play a particularly important role in sensor applications. pH-induced conductance switching has been observed in different types of single-molecule junction where it has been attributed to a molecule undergoing large scale conformational changes[16], breaking of the conjugation of a molecule[17], isomerization[14], or the protonation/de-protonation of a particular functional group within a molecule[7,18,19].

Here we have chosen to investigate Ni|44VDP|Ni junctions since 44VDP (Figure 1a) contains two pH sensitive pyridyl moieties that can be protonated in acidic environments. Compared to the closely related and well-studied molecular conductor 4,4'-bipyridine (44BP)[1,10,20,21], in 44VDP these rings are partly decoupled from each other through the addition of a separating ethylene bridge. Ni contacts were chosen since they have previously been shown to provide an enhanced response to an electrochemically applied gate potential compared with single-molecule junctions formed using Au[1]. We find that the conductance switches between distinct high (on-state) and low (off-state) values as the pH decreases, but in addition the pH at which the conductance switches depends on the electrochemical gate potential. Hence, it is possible to tune a single-molecule-based pH sensor electrically. From the pH and potential dependence of the high and low conductance states we show that the switching is caused by protonation/de-protonation of the pyridine anchor groups of 44VDP resulting in a change in the bonding at the metal-molecule interface. The results also provide insight into the acid-base

equilibrium of single molecules within metal|molecule|metal junctions. In particular, fitting the data to a thermodynamic model of molecular adsorption allowed us to estimate the partial charge transferred to the protonated molecule from the Ni contacts when it forms a junction. Moreover, we observed conductance jumps within individual STM-BJ traces which we interpret as individual proton transfer reactions - of fundamental importance in chemistry[22] - taking place within a single-molecule junction. Our results suggest that the STM-BJ technique could be used more generally to investigate chemical equilibria and reactions at the single-molecule level through dual control of both the environment and the electrochemical potential.
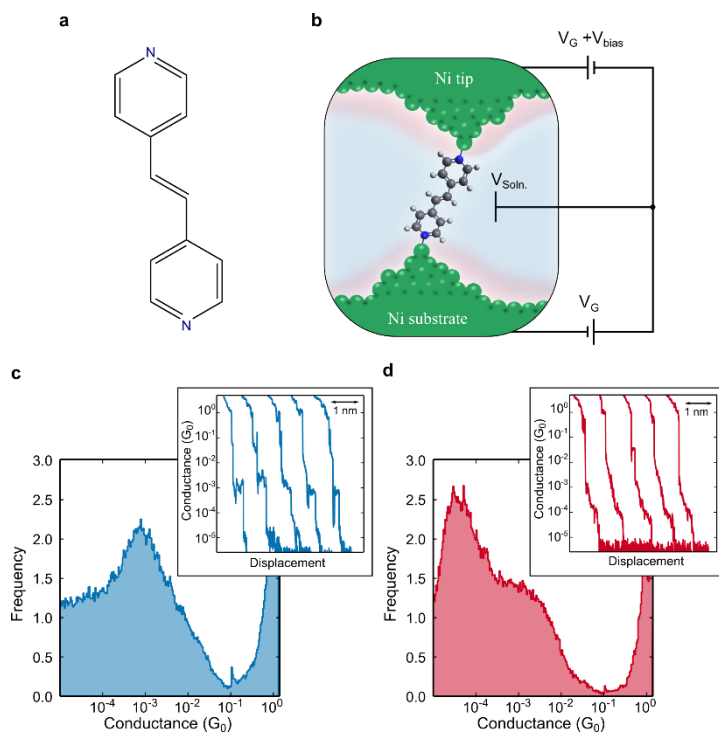

Figure 1. (a) The structure of 4,4'-vinylenedipyridine (44VDP). (b) Schematic representation of the electrochemically controlled STM-BJ technique. The Ni substrate has a potential of V_G applied with respect to the solution (and the molecule) ($V_{Soln.}$), and the tip has a potential difference of V_{bias} (100 mV) with respect to V_G. (c)&(d) Typical conductance histograms

produced without data selection showing the high (containing 1114 traces) and low (containing 850 traces) conductance features measured in a pH 2.85 solution at potentials of -950 and -1150 mV vs. MSE, respectively. The insets show conductance traces (offset laterally for clarity) responsible for producing the conductance features in the corresponding histograms. G_0, the conductance quantum, is equal to $2e^2/h = 7.75 \times 10^{-5}$ S.

The STM-BJ measurements were performed under electrochemical control as shown in Figure 1b. This provides two advantages; firstly it prevents oxidation of the otherwise reactive Ni contacts[1], and secondly an electrochemical gate potential can be applied to the molecular junctions by varying the potential difference between the Ni contacts and the solution [1,3,20,21] (in practice the potential difference between the substrate and a mercury sulfate reference electrode (MSE) is varied whilst the potential between the tip and substrate remains fixed).

Figure 1c and Figure 1d compare the distinct high and low conductance states observed for the Ni|44VDP|Ni junctions at different values of pH and potential. Figure 1c shows a typical conductance histogram for the high conductance state which contains a peak centred at approximately 10^{-3} G_0 (where G_0 is the conductance quantum, equal to $2e^2/h = 7.75 \times 10^{-5}$ S). In Figure 1d on the other hand the dominant peak is located approximately an order of magnitude lower in conductance near 10^{-4} G_0, although the high conductance peak is still apparent. Typical conductance vs. distance traces responsible for producing these features are displayed in the insets to Figure 1c and Figure 1d. Conductance histograms obtained at additional combinations of pH and potential are presented in the Supporting Information (Figure S1). 2-dimensional conductance vs. distance histograms show that the high and low conductance states extend to similar tip separations (Figure S2) and an automated data analysis procedure (see Supporting Information) yielded comparable average molecular plateau lengths for the two states (Figure

S6). These suggest that the physical configuration of the high and low conductance states is similar.
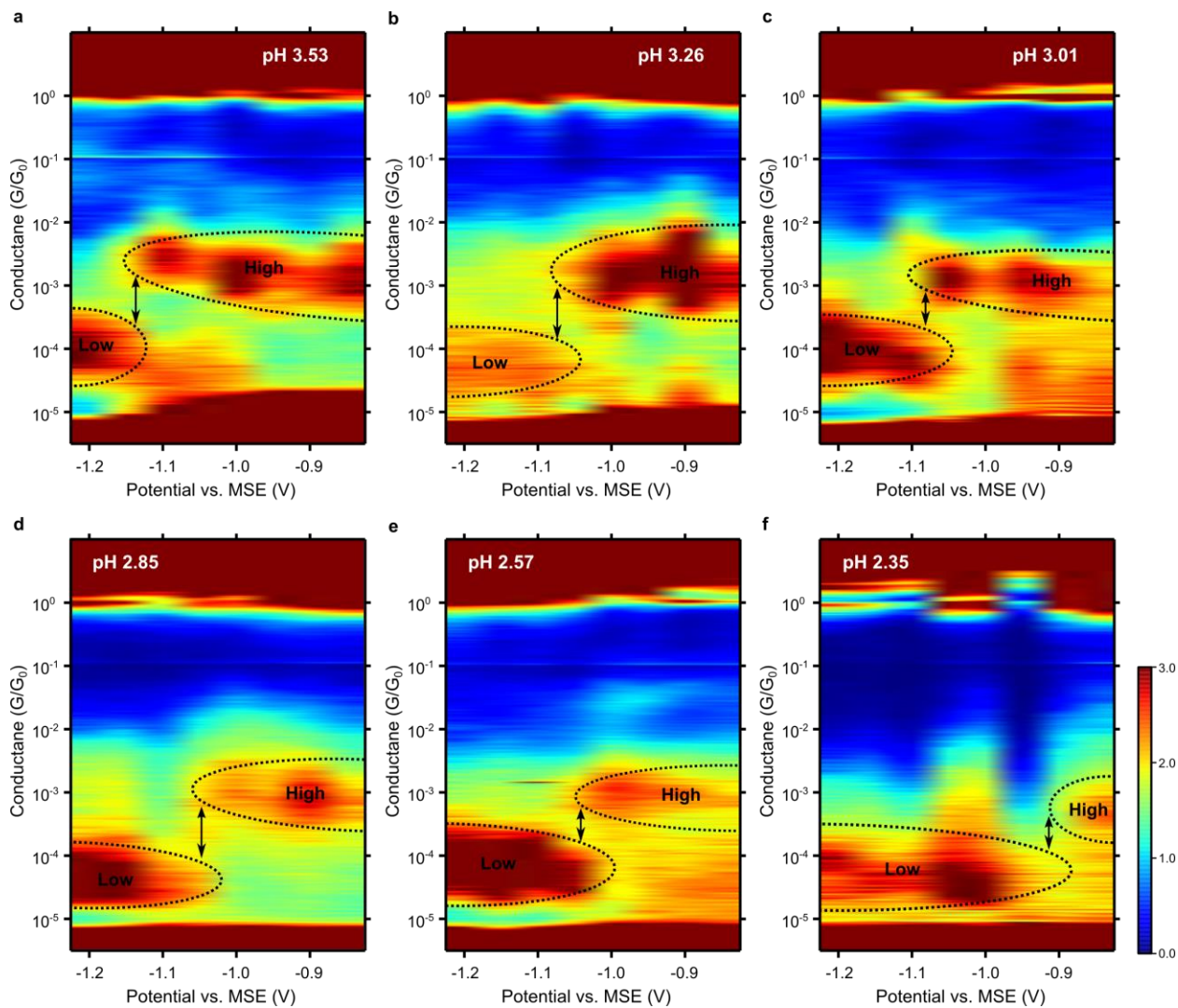

Figure 2. 2-dimensional conductance vs. potential histograms measured for different values of solution pH; (a) pH 3.53, (b) pH 3.26, (c) pH 3.01, (d) pH 2.85, (e) pH 2.57 and (f) pH 2.35. The approximate locations of the high and low conductance states are indicated by the dotted lines. The colour scale represents the number of data points within each 2-dimensional bin normalised to the number of conductance traces in the experiment. The number of traces recorded at each

value of the potential at any particular pH is noted in the Supporting Information (typically between 500 and 1000 traces were recorded).

Figure 2 illustrates the interplay between the pH and the electrochemical gate potential using 2-dimensional (conductance vs. potential) gating histograms. These were constructed (without data selection) from break-junction traces measured at 8 different potentials for each pH value. Each 2-dimensional histogram shows how the conductance evolves as a function of the gate potential for a particular value of the pH. The relative occurrence of different conductance values at each potential is indicated by the colour scale, with high occurrence represented in red and low occurrence in blue. Separate high and low conductance regions, which are clearly distinguishable, are indicated in each panel. At each pH the histograms tend to exhibit the low conductance feature when the substrate is more negative, whilst at more positive potentials the high conductance feature is favoured. The transition from high to low conductance takes place at more positive potentials as the pH is lowered. In other words, the Ni|44VDP|Ni single-molecule junction acts as a pH-dependent switch and the value of the pH at which the conductance switches can be tuned via the gate potential.

The dependence on pH suggests that the conductance switching in Ni|44VDP|Ni molecular junctions is caused by the presence or absence of protons in the vicinity of the molecular junction. Previous measurements of 44BP molecules contacting Ni electrodes did not exhibit conductance switching in the same potential range[1], so the switching is not due to the Ni contacts undergoing some independent chemical or morphological change. On the other hand, the 44VDP molecule contains two pyridyl C_5H_4N moieties that can be protonated to $C_5H_4NH^+$ (44BP also contains these moieties, but the different molecular backbone leads to lower pKa values[23,24] meaning they are only likely to be protonated at lower pH and more negative potentials that are

outside our current experimental range). The pyridyl moieties are the anchor groups that provide contact to the Ni electrodes, so their protonation is extremely likely to change the conductance. A comparison of the conductance of 44VDP molecules contacting Au electrodes measured in a pH 2.5 0.05 M Na_2SO_4 electrolyte under electrochemical control with the conductance measured in a nonpolar solvent (1,3,5-trimethylbenzene) shows that non-protonated junctions can be formed even at pH values lower than the pKa of the molecule (see Supporting Information). Since the high conductance state is observed at higher pH, we attribute it to non-protonated 44VDP, while because the low conductance feature is observed at lower pH, we attribute it to (singly-)protonated 44VDP.   Further analysis of the data using an automated data selection procedure revealed substructure within the low conductance peak which we attribute to protonation of VDP's second pyridyl group (see SI).

   The explanation of the high/low conductance switching in terms of protonated and non-protonated VDP is also consistent with the dependence on potential. Electrostatic considerations mean that more negative gate potentials, corresponding to more negatively charged electrodes, should favour the formation of junctions with positively charged protonated molecules, as indeed is observed. It might seem surprising that protonated 44VDP could form junctions with Ni at all, but there is evidence from the literature that protonated 44BP adsorbs to Cu under electrochemical control [25], and that self-assembled monolayers of *n*-alkylamines arranged on an Au surface contain a mixture of molecules with $–NH_2$ and $–NH_3^+$ binding groups [26], both of which suggest that a protonated 44VDP molecule would be capable of forming a bond with Ni contacts. Furthermore, we can use chemical thermodynamics to obtain the expected relationship between the pH and potential at which protonation occurs, and show that it fits our conductance

data extremely well. For a simplified picture in which adsorbed 44VDP undergoes only a single protonation, the reaction at the surface is

$$44VDPH^{a+}(ads.) \rightleftharpoons 44VDP(ads.) + H^+ + (1-a)e^- \tag{1}$$
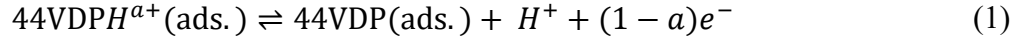
where the protonated 44VDP molecule ($44VDPH^{a+}$) retains a fractional charge of +a after being adsorbed to the Ni surface due to the reorganisation of charges at the interface. Assuming Langmuir behaviour of the adsorbed species it can be shown that the surface concentration Γ of the protonated and non-protonated molecules in the junction follows [27]

$$\log \frac{\Gamma_{VDP}}{\Gamma_{VDPH^{a+}}} = \frac{(1-a)F}{RT \ln(10)}(E - E^0) + \text{pH} \tag{2}$$

where R is the ideal gas constant, F is the Faraday constant, E is the applied potential, and E^0 is the standard potential.
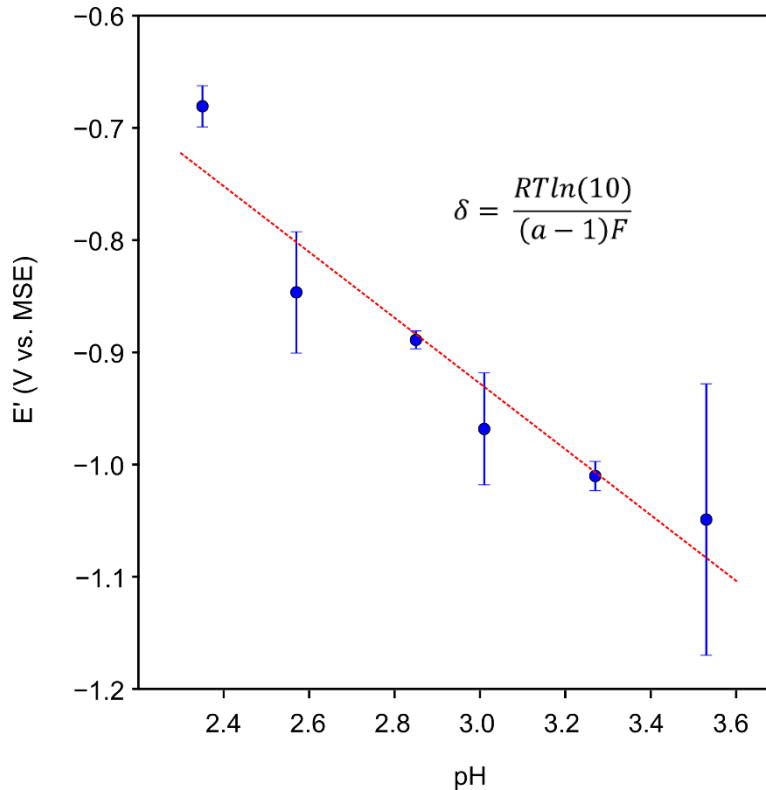
Figure 3. The value of the potential at which equal numbers of protonated and non-protonated junctions form, plotted as a function of pH. The linear fit to the data has a gradient δ where δ = -290±20 mV per pH unit. From Equation 2 we show (see Supporting Information) that δ can be used to calculate a, the charge retained by a protonated 44VDP molecule adsorbed to Ni electrodes as $a = +(0.79 \pm 0.06)\, e$, where e is the charge of an electron.

We determined the relative probability P_{high}/P_{low} of finding the high and low conductance states respectively, as a function of pH and potential using an automated data selection process (see Supporting Information) to distinguish between individual STM-BJ traces containing high and low conductance features. We then used this data to determine the potential E' for which $P_{high}/P_{low} = 1$ for each pH value investigated. Assuming that the high and low conductances correspond to the non-protonated and protonated molecule respectively, and that the probability of forming a junction with each form of the molecule is proportional to its surface concentration Γ, it can be shown that equation (2) implies that E' is proportional to pH (see Supporting Information). Figure 3 shows that this is indeed the case. The excellent agreement between the model and the data strongly supports our interpretation of the high and low conductance states. It further suggests that the local increase in pH caused by hydrogen evolution at the Ni substrate is too small to affect the results significantly. However, we would expect surface pH changes to become important for Ni potentials more negative than -1.2 V vs. MSE[28]. In addition, the gradient of the fitted line δ enables us to estimate that a = (0.79 ± 0.06) e, corresponding to the transfer of a partial negative change from the nickel contacts to a positively charged protonated 44VDP molecule (i.e. the net charge on the molecule is +a, rather than +1). The value of a will be a key input for future theoretical investigations of this novel charged molecular junction.

In addition to the STM-BJ traces discussed so far, where either a high or low conductance feature was observed, some were found to exhibit clear switching between the high and low conductance states during a single trace. Figure 4 shows typical traces in which switching events occur. Switching between high and low conductance levels can be clearly observed and in some cases multiple switching events occur within a single trace. The obvious explanation is that they are due to individual protonation and de-protonation reactions occurring at a single molecule. It is remarkable that these can now be observed in real time using the STM-BJ technique [29]. In particular the fact that multiple switches can be observed during an individual trace suggests that the switching is stochastic, which is consistent with the idea that it is driven by chemical interaction rather than by structural rearrangements caused e.g. by the junction stretching. The ability to detect such processes at the single-molecule level promises to provide insight into chemical reactions which is unobtainable through typical ensemble techniques [29–31].
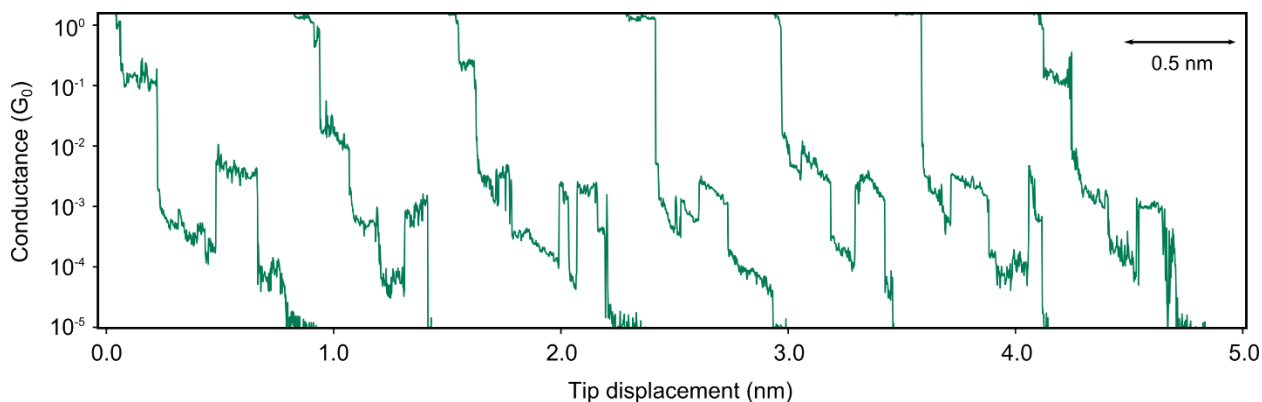

Figure 4. Typical conductance vs. distance traces with stochastic switching between the high and low conductance states of Ni|44VDP|Ni. The traces have been offset laterally for clarity.

In conclusion, we measured the conductance of Ni|44VDP|Ni single-molecule junctions using an electrochemically controlled STM-BJ technique and found that these switched between high

and low conductance states depending on both the solution pH and the electrochemical gate voltage. We attribute the switching of these devices to a change in the molecule-electrode contact caused by protonation of the 44VDP in the junction at low pH values and negative potentials. The observation of switching events within single STM-BJ traces implies that individual proton transfer reactions can now be detected in real time. Furthermore, the transition between high and low conductance states could be utilized in a pH-sensitive switch. Crucially, the pH at which the switching takes place can be tuned using a gate voltage, so that the Ni|44VDP|Ni junctions constitute a three-terminal sensor where the input to the gate electrode determines the level of stimulus at which the device responds. Hence, in principle, this sensor could be used not only to detect pH changes but to measure the local pH.

ASSOCIATED CONTENT

Supporting Information. Additional information on experimental methods and supporting results and figures. This material is available free of charge via the Internet at http://pubs.acs.org/.

AUTHOR INFORMATION

Corresponding Author

* E-mail: w.schwarzacher@bristol.ac.uk.

Author Contributions

R.J.B. carried out the measurements and analysed the data. D.S.S. developed the apparatus used in STM-BJ experiments. R.J.N and W.S. designed the project. All authors contributed to the interpretation of the results and to preparation of the manuscript.

Notes

The authors declare no competing financial interest.

REFERENCES

(1)   Brooke, R. J.; Jin, C.; Szumski, D. S.; Nichols, R. J.; Mao, B.-W.; Thygesen, K. S.; Schwarzacher, W. *Nano Lett.* **2015**, *15* (1), 275–280.

(2)   Perrin, M. L.; Burzurí, E.; van der Zant, H. S. J. *Chem. Soc. Rev.* **2015**, *44* (4), 902–919.

(3) Osorio, H. M.; Catarelli, S.; Cea, P.; Gluyas, J. B. G.; Hartl, F.; Higgins, S. J.; Leary, E.; Low, P. J.; Martín, S.; Nichols, R. J.; Tory, J.; Ulstrup, J.; Vezzoli, A.; Milan, D. C.; Zeng, Q. *J. Am. Chem. Soc.* **2015**, *137* (45), 14319–14328.

(4) Vezzoli, A.; Brooke, R. J.; Ferri, N.; Higgins, S. J.; Schwarzacher, W.; Nichols, R. J. *Nano Lett.* **2017**, *17* (2), 1109–1115.

(5) Capozzi, B.; Xia, J.; Adak, O.; Dell, E. J.; Liu, Z.-F.; Taylor, J. C.; Neaton, J. B.; Campos, L. M.; Venkataraman, L. *Nat. Nanotechnol.* **2015**, *10* (6), 522–527.

(6) Batra, A.; Darancet, P.; Chen, Q.; Meisner, J. S.; Widawsky, J. R.; Neaton, J. B.; Nuckolls, C.; Venkataraman, L. *Nano Lett.* **2013**, *13* (12), 6233–6237.

(7) Morales, G. M.; Jiang, P.; Yuan, S.; Lee, Y.; Sanchez, A.; You, W.; Yu, L. *J. Am. Chem. Soc.* **2005**, *127* (30), 10456–10457.

(8) Milan, D. C.; Al-Owaedi, O. A.; Oerthel, M.-C.; Marqués-González, S.; Brooke, R. J.; Bryce, M. R.; Cea, P.; Ferrer, J.; Higgins, S. J.; Lambert, C. J.; Low, P. J.; Manrique, D. Z.; Martin, S.; Nichols, R. J.; Schwarzacher, W.; García-Suárez, V. M. *J. Phys. Chem. C* **2016**, *120* (29), 15666–15674.

(9) Milan, D. C.; Krempe, M.; Ismael, A. K.; Movsisyan, L. D.; Franz, M.; Grace, I.; Brooke, R. J.; Schwarzacher, W.; Higgins, S. J.; Anderson, H. L.; Lambert, C. J.; Tykwinski, R. R.; Nichols, R. J. *Nanoscale* **2017**, *9* (1), 355–361.

(10) Quek, S. Y.; Kamenetska, M.; Steigerwald, M. L.; Choi, H. J.; Louie, S. G.; Hybertsen, M. S.; Neaton, J. B.; Venkataraman, L. *Nat. Nanotechnol.* **2009**, *4* (4), 230–234.

(11) Zhang, W.; Gan, S.; Vezzoli, A.; Davidson, R. J.; Milan, D. C.; Luzyanin, K. V.; Higgins, S. J.; Nichols, R. J.; Beeby, A.; Low, P. J.; Li, B.; Niu, L. *ACS Nano* **2016**, *10* (5), 5212–5220.

(12) Perrin, M. L.; Frisenda, R.; Koole, M.; Seldenthuis, J. S.; Gil, J. A. C.; Valkenier, H.; Hummelen, J. C.; Renaud, N.; Grozema, F. C.; Thijssen, J. M.; Dulić, D.; van der Zant, H. S. J. *Nat. Nanotechnol.* **2014**, *9* (10), 830–834.

(13) Martin, S.; Haiss, W.; Higgins, S. J.; Nichols, R. J. *Nano Lett.* **2010**, *10* (6), 2019–2023.

(14) Darwish, N.; Aragonès, A. C.; Darwish, T.; Ciampi, S.; Díez-Pérez, I. *Nano Lett.* **2014**, *14* (12), 7064–7070.

(15) Bruot, C.; Hihath, J.; Tao, N. *Nat. Nanotechnol.* **2011**, *7* (1), 35–40.

(16) Scullion, L.; Doneux, T.; Bouffier, L.; Fernig, D. G.; Higgins, S. J.; Bethell, D.; Nichols, R. J. *J. Phys. Chem. C* **2011**, *115* (16), 8361–8368.

(17) Li, Z.; Smeu, M.; Afsari, S.; Xing, Y.; Ratner, M. A.; Borguet, E. *Angew. Chemie Int. Ed.* **2014**, *53* (4), 1098–1102.

(18) Li, L.; Lo, W.-Y.; Cai, Z.; Zhang, N.; Yu, L. *Chem. Sci.* **2016**, *7* (5), 3137–3141.

(19) Xiao; Xu, and; Tao, N. *J. Am. Chem. Soc.* **2004**, *126* (17), 5370–5371.

(20) Baghernejad, M.; Manrique, D. Z.; Li, C.; Pope, T.; Zhumaev, U.; Pobelov, I.; Moreno-García, P.; Kaliginedi, V.; Huang, C.; Hong, W.; Lambert, C.; Wandlowski, T. *Chem. Commun. (Camb)*. **2014**, *50* (100), 15975–15978.

(21)   Capozzi, B.; Chen, Q.; Darancet, P.; Kotiuga, M.; Buzzeo, M.; Neaton, J. B.; Nuckolls, C.; Venkataraman, L. *Nano Lett.* **2014**, *14* (3), 1400–1404.

(22)   Eigen, M.; Kruse, W.; Maass, G.; DeMaeyer, L. *PROG. REACT. KINET. MEC.* **1964**, *2*, 285–318.

(23)   Musgrave, T. R.; Mattson, C. E. *Inorg. Chem.* **1968**, *7* (7), 1433–1436.

(24)   Israeli, M.; Laing, D. K.; Pettit, L. D. *J. Chem. Soc. Dalt. Trans.* **1974**, No. 20, 2194.

(25)   Diao, Y.-X.; Han, M.-J.; Wan, L.-J.; Itaya, K.; Uchida, T.; Miyake, H.; Yamakata, A.; Osawa, M. *Langmuir* **2006**, *22* (8), 3640–3646.

(26)   de la Llave, E.; Clarenc, R.; Schiffrin, D. J.; Williams, F. J. *J. Phys. Chem. C* **2014**, *118* (1), 468–475.

(27)   Martínez-Hincapié, R.; Berná, A.; Rodes, A.; Climent, V.; Feliu, J. M. *J. Phys. Chem. C* **2016**, *120* (29), 16191–16199.

(28)   Deligianni, H.; Romankiw, L. T. *IBM J. Res. Dev.* **1993**, *37* (2), 85–95.

(29)   Xiang, L.; Palma, J. L.; Li, Y.; Mujica, V.; Ratner, M. A.; Tao, N. *Nat. Commun.* **2017**, *8*, 14471.

(30)   Mattei, M.; Kang, G.; Goubert, G.; Chulhai, D. V.; Schatz, G. C.; Jensen, L.; Van Duyne, R. P. *Nano Lett.* **2017**, *17* (1), 590–596.

(31)   Aragonès, A. C.; Haworth, N. L.; Darwish, N.; Ciampi, S.; Bloomfield, N. J.; Wallace, G. G.; Diez-Perez, I.; Coote, M. L. *Nature* **2016**, *531* (7592), 88–91.

TABLE OF CONTENTS GRAPHIC